Raman and resonance Raman investigation of MoS_2 nanoparticles

Gitti L. Frey and Reshef Tenne
Department of Materials and Interfaces, Weizmann Institute, Rehovot 76100, Israel

Manyalibo J. Matthews and M. S. Dresselhaus
Department of Physics, Massachusetts Institute of Technology, Cambridge, Massachusetts 02139

G. Dresselhaus
Francis Bitter Magnet Laboratory, Massachusetts Institute of Technology, Cambridge, Massachusetts 02139
(Received 22 January 1999)

Raman and resonance Raman spectra of MoS_2 nanoparticles, in the form of inorganic fullerenelike nanoparticles with diameters ranging from 200 to 2000 Å in size, and platelets ranging from 50 to 5000 Å in size, are presented. Off resonance, the first-order Raman bands are broadened, but not significantly shifted, and no additional bands are observed, indicating that the atomic structure is preserved, at least locally, in the nanoparticles. The broadening effect is assigned to phonon confinement by facet boundaries. In the resonance Raman spectra of the nanoparticles, several additional first-order peaks are observed. The electron-phonon coupling responsible for the strong-resonance conditions is identified through dynamic band calculations. Using temperature-dependent resonance Raman measurements, we assign these peaks to zone-boundary phonons activated by disorder and finite-size effects. By analyzing the position of the dispersive peak at 429 cm^{-1} under resonance conditions, it was possible to probe the softening of modes propagating in the *c*-axis direction. [S0163-1829(99)08827-X]

INTRODUCTION

Nanocrystalline and microcrystalline semiconductors have become an interesting topic of study since their optical and electronic properties differ from those of their corresponding single crystals. While the atomic structure and chemical bonds in the nanocrystals are similar to those of the single crystal, their unique properties originate from their size. In the nanometer-size regime, the optical, electrical, magnetic, chemical, and mechanical properties become a function of nanoparticle size. These properties could thus be tuned by synthesizing size-selective particles.[1,2] However, controlling not only the size, but also the structure of a nanoparticle, would extend the tailoring capabilities and would generate additional unique properties. Carbon nanotubes have been, in particular, the subject of numerous size-structure-property relation studies.[3]

Following the discovery of C_{60}, carbon nanotubes and graphitic onionlike polyhedra, it was suggested that under suitable conditions, other layered compounds would form similar closed structures. The semiconducting-layered compounds MoS_2 and WS_2 were the first inorganic fullerenelike (IF) and nanotube structures obtained.[4–8] Since IF-MS_2 (M = Mo; W) particles are chemically inert and stable at temperatures up to 300 °C, they have shown promise for use as solid lubricants.[9] Furthermore, MS_2 nanotubes display interesting electronic and optical properties that make them promising materials as probes for scanning probe microscopy techniques. Therefore, these materials are attractive systems to study in the context of ''structure-property'' relationships in nanomaterials.

In this paper, we present a Raman and resonance Raman study of MoS_2 nanoparticles in the form of fullerenelike (IF) and platelet (PL) samples and compare the results to those of MoS_2 single crystals. Resonance Raman (RR) scattering can be used as a sensitive probe to monitor changes in the electronic states of the system brought about by quantum confinement or synthesis-specific structural modifications in these nanoparticles. We study both the phonon structure and the electron-phonon coupling in MoS_2 nanoparticles by Raman, resonance Raman, and dynamic electronic band-structure calculations.

BACKGROUND

IF-MoS_2 particles have been previously investigated by x-ray powder diffraction (XRD),[10] scanning tunneling microscopy,[11] high-resolution transmission electron microscopy (TEM),[10,12,13] and optical-absorption spectroscopy.[14] The XRD analysis revealed that the bulk $2H$ structure of the unit cell is locally preserved within an IF particle. Nonetheless, a shift of the XRD (0002) peak of the IF phase indicates a lattice expansion of ~2% between two adjacent MS_2 slabs along the c axis compared to its bulk $2H$ polytype.[10] $2H$ bulk MoS_2 is a semiconductor with indirect and direct band gaps at room temperature of 1.2 and 1.95 eV, respectively.[14] The absorption edge consists of two exciton series, A and B, at 1.88 and 2.06 eV, respectively.[15,16] These excitons are assigned to transitions at the K point of the Brillouin zone, with K_4 and K_1 being the initial states, and K_5 the final state.[15] A systematic study of the optical properties of IF-MS_2 shows that the semiconductivity of the layered material is preserved in the IF structures. However, a decrease (redshift) in the band gap[11] and exciton energies[14] of the IF compared to the $2H$ bulk is found. For IF-MoS_2 (value for $2H$ bulk in parentheses) at room temperature, the A and B

exciton energies are 1.82 (1.88) and 1.95 (2.06) eV, respectively. No similar redshift is observed for PL-MoS_2. Such modifications of the electronic structure are believed to be related to the structural changes necessary to form an IF structure. Evidence for two-dimensional (2D) quantum confinement, in the direction perpendicular to the layers ($\|c$), is found for IF particles with less than 5 layers.[14] PL-MoS_2 samples exhibit quantum confinement[17] when their size decreases below 200 Å.

The Raman spectra of bulk $2H$ MoS_2 have been studied extensively.[18,20] A group-theoretical analysis of the lattice vibrations in $2H$ MoS_2 at the Γ point in the hexagonal Brillouin zone (BZ) has been previously published.[19] There are four Raman-active modes in bulk $2H$ MoS_2, corresponding to the following symmetries (with measured frequencies in parentheses): $E^2_{2g}(32\,\mathrm{cm}^{-1})$, $E_{1g}(286\,\mathrm{cm}^{-1})$, $E^1_{2g}(383\,\mathrm{cm}^{-1})$, and $A_{1g}(408\,\mathrm{cm}^{-1})$. The E^2_{2g} phonon is associated with the vibration of an MS_2 layer against neighboring layers and is called the rigid-layer mode. In backscattering experiments on a surface perpendicular to the c axis, the $E_{1g}(286\,\mathrm{cm}^{-1})$ mode is forbidden. The RR spectrum of bulk $2H$ MoS_2 has been previously reported using laser energies near the absorption edge.[20–22] The RR scattering of bulk $2H$ MoS_2 has been analyzed in terms of both zone-center first-order Raman scattering (FOR) and second-order Raman (SOR) scattering enhanced by the coupling of phonon modes to electronic transitions associated with the excitonic states.[21] An intense SOR band at 460 cm^{-1} is observed, and is due to a second-order $2\times\mathrm{LA}(M)$ scattering process, while other SOR peaks are assigned to sum or difference bands involving other phonons at the M point coupled to the LA(M) mode.[19,21] If the exciting laser line is just above the $1s$ level of the A exciton, an additional peak appears at $\sim$430 cm^{-1} (''b'' peak in Ref. 20) which shifts to lower frequencies as the energy of the exciting laser increases.[20] This peak has been interpreted in terms of a two-phonon Raman process involving the successive emission of a dispersive longitudinal quasiacoustic phonon and a dispersionless E^2_{1u} phonon, both along the c axis.[20]

EXPERIMENT

The synthetic method for preparing IF- and PL- MoS_2 nanoparticles has been previously published.[10,12,13] Briefly, a starting precursor of MoO_3 powder is heated to temperatures above 800 °C and is reduced to MoO_{3-x} in a reducing atmosphere (typically 5%H_2/95%N_2). The suboxide sublimes and reacts with H_2S gas, which converts the suboxide particle into the corresponding MS_2 nanoparticle.[10] The reaction product is collected in powder form on a quartz substrate and is characterized by XRD and TEM. Two distinct growth regimes can lead to either IF or PL nanoparticles.[10]

Raman spectra were recorded at ambient temperatures using a standard backscattering geometry. Excitation wavelengths of 4880 and 5145 Å (2.54 and 2.41 eV, respectively) were produced by an argon ion laser source capable of supplying 20–100 mW of power. In order to prevent damage to the samples, an optical filter was used to reduce the incident power to roughly 0.6 mW. Several locations on each sample surface were probed to ensure reproducibility of the data. The scattered light was focused into a double grating monochromator fitted with a 300-μm slit. Scattering intensities were measured using a high-resolution charge coupled device (CCD) camera. For the resonance Raman (RR) spectra, the 6328 Å (1.96 eV) line of a He/Ne laser was used, capable of supplying 1 mW of power. Several locations of each sample surface were probed to ensure reproducibility of the data. Scattering intensities were measured using a high-resolution CCD camera. For low-temperature measurements, a continuous flow liquid-nitrogen-cooled cold plate equipped with an optical window was used. Both Stokes and anti-Stokes scattering intensities were measured in order to accurately determine the sample temperature.

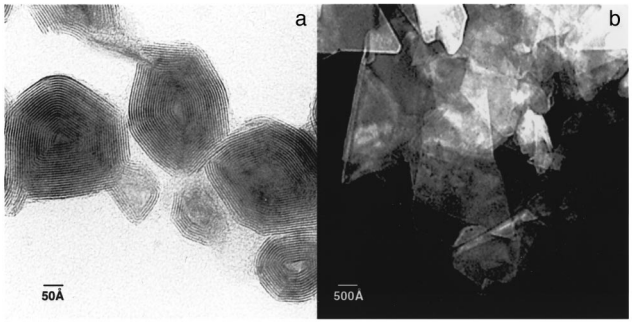

FIG. 1. TEM micrograph of (a) a typical IF-MoS_2 particle [the distance between two fringes (MoS_2 layers) is 6.2 Å] and (b) a typical sample of MoS_2 nanosize clusters in the form of platelets (PL).

Electronic dynamic band-structure calculations of a MoS_2 single layer were performed using an ''extended-Hückel approximation'' procedure.[23,24] Dynamic band calculations are done by displacing the atomic positions in the direction of a specific phonon and recalculating the electronic band structure. The direct and indirect band gaps are extracted graphically from the calculated band structures. Thus, the dynamic electronic band-structure calculations probe the electron-phonon coupling.

RESULTS

Sample characterization by TEM

The examination of large series (>1000) of MX_2 nanoparticles by TEM shows that the synthesis of both IF and PL structures yields particles with diameters ranging from 200 to 2000 Å and from 50 to 5000 Å, respectively. Furthermore, the micrographs reveal that the structure of IF-MX_2 may be described in terms of a relatively large number of low-angle grain boundaries or by a uniform array of dislocations.[25] Figures 1(a) and 1(b) show TEM micrographs of typical IF-MoS_2 and PL-MoS_2 particles, respectively. The IF nanoparticles shown in Fig. 1 are $\sim$300 Å in diameter and contain 15 to 20 sulfide layers. They are faceted, with very flat atomic planes, ranging from 70 to 250 Å in length, joined at sharply defined grain boundaries. Examination of samples containing larger IF particles (pictures not shown) revealed that, although the length of the facets increase with increasing IF size, the facet lengths do not exceed 350 Å. Fre-

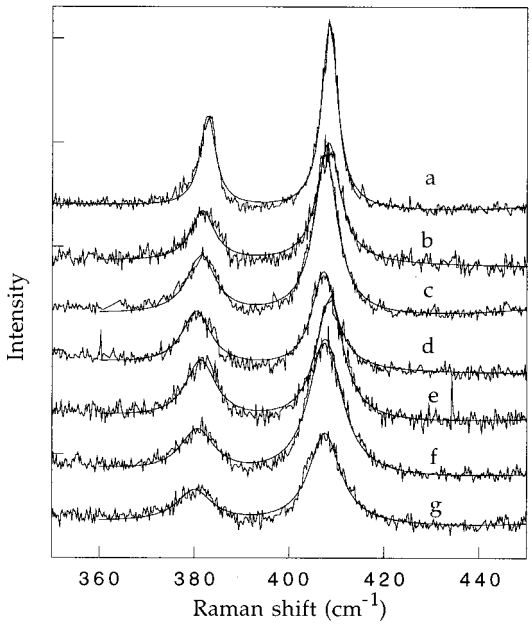

FIG. 2. Raman spectra excited by the 4880-Å (2.54 eV) laser line of several MoS_2 nanoparticle samples: PL-MoS_2 5000 Å (curve *a*); PL-MoS_2 200×500 Å^2 (curve *b*); IF-MoS_2 1000–1500 Å (curve *c*); IF-MoS_2 800 Å (curve *d*); PL-MoS_2 50×300 Å^2 (curve *e*); IF-MoS_2 200 Å with 10–15 sulfide layers (curve *f*); IF-MoS_2 200 Å with 5–10 sulfide layers (curve *g*).

quently in the large IF nanoparticles, the inner layers are faceted while the outer layers are continuous and fairly spherical.[25] The Raman spectra were recorded on films containing over 90% of a single phase of the nanoparticles, with a 10% size distribution of the nanoparticles.

Raman scattering

The off-resonance Raman spectra excited at 4880 Å (2.54 eV) of IF- and PL-MoS_2 of various sizes and numbers of sulfide layers are shown in Fig. 2 and compared to the corresponding spectra for the single crystal. Two strong Raman peaks are observed at 383 and 408 cm^{-1}, which correspond to the $2H$ MoS_2 E^1_{2g} and A_{1g} modes, respectively. The frequencies of these peaks are identical in the spectra of the nanoparticles and the single crystal. Nevertheless, a least-squares fit reveals that the modes are broadened in the spectra of the nanoparticles. The full width at half maximum (FWHM) intensity of both peaks increases from roughly 4 cm^{-1} for the 5000-Å platelets to 9 cm^{-1} for the 200-Å IF sample. The relative intensities of the A_{1g} to E^1_{2g} peaks do not vary significantly from one curve to another. The Raman spectra of IF-MoS_2 and PL-MoS_2 excited with the 5145-Å (2.41-eV) laser line show similar features to those obtained by the 4880-Å line regarding both the peak broadening and relative intensities.

Resonance Raman scattering

Resonance Raman (RR) scattering of MoS_2 is obtained by exciting the samples with the He/Ne 6328-Å laser line (1.96 eV) which is in resonance with the direct band gap (1.96 eV). Figures 3(a) and 3(b) show the RR spectra of MoS_2 samples at 300 and 125 K, respectively. The frequencies of the modes shown in Fig. 3 are listed in Table I and Table II. Under resonance conditions, the two first-order modes observed off resonance are still broadened in the spectra of the nanoparticles, but their relative intensities vary between samples. In addition, new features are observed in the RR spectra of both single crystal and nanoparticles relative to their corresponding off-resonance spectra.

In contrast to the off-resonance scattering spectra, the intensity of the A_{1g} mode is enhanced under resonance conditions and the relative intensities of the A_{1g} to E^1_{2g} peaks increase for all samples. In the RR spectra of the nanoparticles [curves *a*–*c* in Fig. 3(a)], this relative intensity is larger than that observed for the single crystal [curve *e* in Fig. 3(a)]. At 125 K, on the other hand, it is the E^1_{2g} mode that is enhanced in the spectra of the nanoparticles [curves *a*–*c* in Fig. 3(b)].

In the dynamic band calculations, the atomic positions are displaced in the direction of the E^1_{2g} or A_{1g} phonons. After each displacement, the electronic band structure is recalculated and the indirect and direct transitions are deduced. A few of the calculated band structures are presented in Fig. 4, and the calculated electronic transitions are summarized in Table III. The dynamic calculations show that when ''applying'' the A_{1g}-mode displacements to the material, both the direct and indirect gaps are strongly modulated. On the other hand, the E^1_{2g}-mode displacements modulate the electronic structure only slightly.

In the room-temperature RR spectrum of MoS_2 single crystal [curve *e* in Fig. 3(a)] compared to that obtained off resonance, many peaks are observed. The most intensive peak is asymmetric and centered at ~460 cm^{-1}. This mode has been previously assigned by Stacy *et al.*[21] to the second-order $2\times\mathrm{LA}(M)$ mode. In the spectra of the 5000-Å platelets [curve *d* in Fig. 3(a)], this peak is actually split, suggesting that this feature is a superposition of two peaks. Figure 5 shows a line-shape analysis of this feature revealing two overlapping peaks centered at 457 and 468 cm^{-1}. A similar line-shape analysis was fitted to the RR spectra of different MoS_2 samples and the results are presented in Table IV. The positions of the deconvolved peaks do not vary much from one sample to another or as the temperature is varied. Nevertheless, the integrated relative intensity of the components (~455 cm^{-1}/~466 cm^{-1}), (fourth column in Table IV) at room temperature, increases significantly as the size of the IF and PL particles decreases. The corresponding enhancement of the ~455-cm^{-1} feature in the spectra of the nanoparticles is also observed at 125 K, but is much weaker.

In the higher frequency region of the single-crystal room-temperature RR spectra, peaks are observed at 572, 599, and 641 cm^{-1}, which were assigned by Stacy *et al.*[21] to the second-order processes: $2E_{1g}(\Gamma)$, $E^1_{2g}(M)+\mathrm{LA}(M)$, and $A_{1g}(M)+\mathrm{LA}(M)$, respectively. In the spectra of the smaller particles, the 572- and 599-cm^{-1} features are weak, and, therefore, it is difficult to define their positions accurately. Nevertheless, the 641-cm^{-1} peak shifts to lower energies in the spectra of the nanoparticles. At low temperatures the resolution of these modes is better and their positions are easily determined. In contrast to the room-temperature spectra, the positions of these peaks in the 125-K spectra of the nanoparticles and the single crystal are identical.

Previously, a highly dispersive peak at ~430 cm^{-1} was reported by Sekine *et al.* for MoS_2 single crystal at room temperature,[20] using a wide range of laser energies. For a

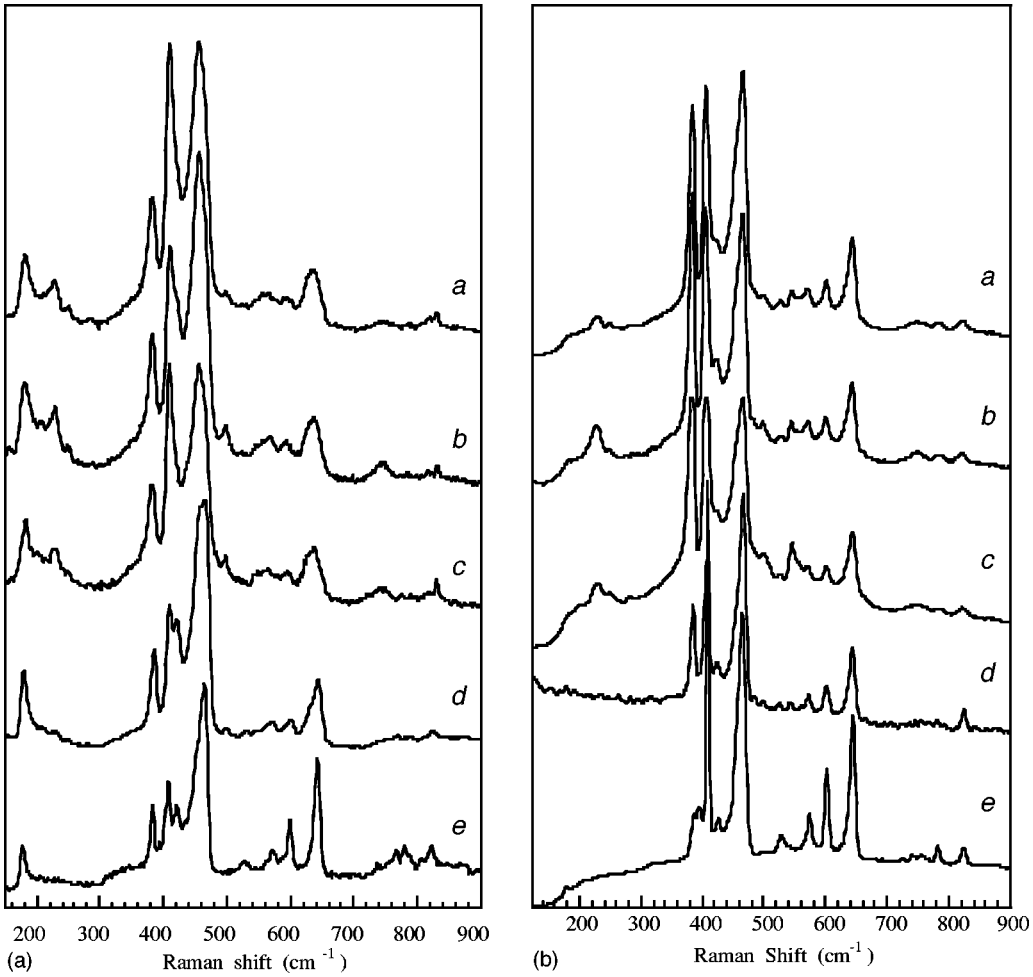

FIG. 3. Resonance Raman (RR) spectra excited by the 6328 Å (1.96 eV) laser line at room temperature (a) and 125 K (b) showing SOR bands of several MoS_2 nanoparticle samples: IF-MoS_2 200 Å (curve *a*); IF-MoS_2 800 Å (curve *b*); PL-MoS_2 50×300 $Å^2$ (curve *c*); PL-MoS_2 5000 Å (curve *d*); bulk 2*H*-MoS_2 (curve *e*).

fixed laser energy of 1.96 eV, this peak is slightly downshifted (relative to the bulk) in the spectra of nanoparticles, and, in some cases, this feature appears as a shoulder or tail of the high-frequency A_{1g} mode. The study by Sekine *et al.*[20] was done only at room temperature, and, therefore, the results at 125 K could not be compared to previous studies.

Finally, in the 300 and 125 K RR spectra of the nanoparticles, peaks are observed at: 226, 247, 495, and 545 cm^{-1}.

TABLE I. Raman peaks observed in the MoS_2 nanoparticle spectra at room temperature and the corresponding symmetry assignments. All peak positions are in cm^{-1}.

Bulk MoS_2[a]	PL-MoS_2 5000 Å	PL-MoS_2 30×50 $Å^2$	IF-MoS_2 800 Å	IF-MoS_2 200 Å	Symmetry assignment
177	179	180	180	179	$A_{1g}(M)-\mathrm{LA}(M)$
		226	227	226	$\mathrm{LA}(M)$
			248	248	
				283	$E_{1g}(\Gamma)$
382	384	381	378	378	$E^1_{2g}(\Gamma)$
407	409	408	407	406	$A_{1g}(\Gamma)$
421[b]	419		weak	weak	
465	460	455	452	452	$2\times\mathrm{LA}(M)$
		498	495	496	Edge phonon
526	529				$E_{1g}(M)+\mathrm{LA}(M)$
		545	545	543	
572	572	~557	565	563	$2\times E_{1g}(\Gamma)$
599	601	595	591	593	$E^1_{2g}(M)+\mathrm{LA}(M)$
641	644	635	633	633	$A_{1g}(M)+\mathrm{LA}(M)$

[a]Reference 12.
[b]Reference 10.

TABLE II. Raman peaks observed in the MoS_2 nanoparticle spectra at 125 K and the corresponding symmetry assignments. All peak positions are in cm^{-1}.

Bulk MoS_2	PL-MoS_2 5000 Å	PL-MoS_2 30×50 Å^2	IF-MoS_2 800 Å	IF-MoS_2 200 Å	Symmetry assignment
					$A_{1g}(M)-\mathrm{LA}(M)$
		230	229	229	$\mathrm{LA}(M)$
			247	249	
				287	$E_{1g}(\Gamma)$
386	384	381	382	383	$E^1_{2g}(\Gamma)$
395					
410	407	407	406	406	$A_{1g}(\Gamma)$
426	423	423	422	422	
465	467	466	465	452	$2\times\mathrm{LA}(M)$
		498	498	499	Edge phonon
529	525	527	528	527	$E_{1g}(M)+\mathrm{LA}(M)$
		545	544	544	
574	573	571	571	571	$2\times E_{1g}(\Gamma)$
602	600	602	600	601	$E^1_{2g}(M)+\mathrm{LA}(M)$
644	644	643	643	644	$A_{1g}(M)+\mathrm{LA}(M)$

These features are not observed in the RR spectra of the single crystal. Possible mechanisms that could bring about these features are discussed below.

DISCUSSION

In this section, we first discuss the broadening and relative intensity of the E^1_{2g} and A_{1g} first-order modes in the Raman and RR spectra of MoS_2 nanoparticles. Next, we discuss possible assignments for the new modes observed in the spectra of the nanoparticles under resonance conditions. Finally, the features observed at ~460 and ~430 cm^{-1} in the RR spectra of both MoS_2 single crystal and nanoparticles are addressed.

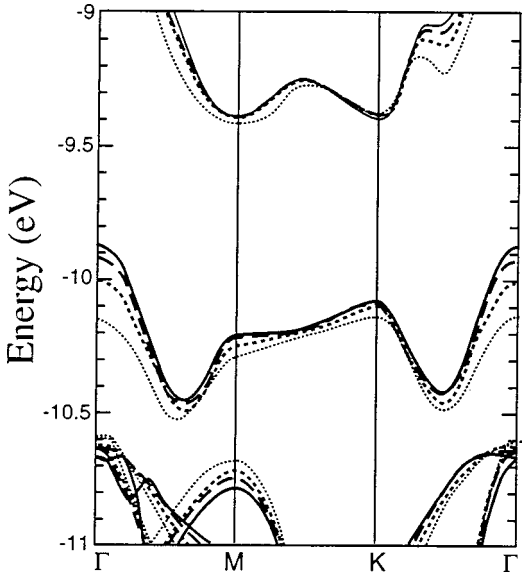

FIG. 4. Calculated electronic band-structure diagrams of a $2H$-MoS_2 single layer after displacing the atomic positions in the direction of the A_{1g} phonon. The band structure of an ordinary $2H$-MoS_2 single layer is presented by the solid lines (——), in this case the Mo-S distance is 2.413 Å and the dihedral angle is 139.11°. (— — —) atomic displacement of 0.02 Å, Mo-S distance is 2.427 Å and the dihedral angle is 139.75°. (----------) atomic displacement of 0.05 Å, Mo-S distance is 2.447 Å and the dihedral angle is 138.22°. (·····) atomic displacement of 0.1 Å, Mo-S distance is 2.480 Å and the dihedral angle is 137.36°.

Raman spectroscopy has been extensively used for the characterization of micro and nanocrystallites including diamond,[26] Si,[27] and GaAs.[27] The obvious differences between the Raman spectra of bulk and micro and nanocrystallites are a frequency shift and a broadening of the Raman bands. A model, known as the spatial-correlation or phonon-confinement model, explains the observed shift to lower frequency and a broadening of the Raman line in microcrystallites.[28,29] Due to crystal momentum conservation, the Raman spectroscopy of ideal large crystals probes phonons at the center of the *Brillouin* zone (BZ) where $q=0$. However, phonons can be confined in space by crystallite boundaries or defects.[28,29] This results in an uncertainty in the phonon momentum, allowing phonons with $(q>0)$ to contribute to the Raman signal. According to the confined-phonon model, the Raman line shape is constructed by superimposing Lorentzian line shapes (with the line widths of the bulk) centered at $\omega(q)$ weighted by the wave vector uncertainty caused by the confinement. A Gaussian is used for the confining function. The resulting Raman line shape is given by[30]

$$I(\omega,\xi)\propto\frac{\xi^3}{\pi^{3/2}}\int dq\,\frac{\exp(-\xi^2q^2)}{[\omega-\omega(q)]^2+(\Gamma/2)^2}, \qquad (1)$$

where $\omega(q)$ is the phonon-dispersion curve, Γ is the FWHM of the Raman line observed in the bulk, and ξ is the assumed Gaussian correlation length, which is proportional to the crystallite size L (frequently used: $\xi=L/2$).

Assuming that the broadening of the first-order modes for the IF and PL samples in Fig. 2 is due to phonon confinement, we use Eq. (1) to calculate the Raman line shape for the IF and PL samples. Since the experimental phonon dispersion curve function $\omega(q)$ is not available for the MoS_2

TABLE III. Atomic displacement and calculated direct and indirect transitions.

	A_{1g} Mode		E^1_{2g} Mode	
Atomic displacement Å	Γ-K (eV) indirect transition	K-K (eV) direct transition	Γ-K (eV) indirect transition	K-K (eV) direct transition
0	0.47	0.69	0.48	0.68
0.02	0.50	0.69	0.48	0.68
0.04	0.61	0.72	0.48	0.68
0.05	0.63	0.73	0.48	0.68
0.06	0.66	0.75	0.49	0.68
0.08	0.71	0.76	0.49	0.68
0.1	0.79	0.78	0.49	0.67

system, we use the dispersion plots calculated by Wakabayashi *et al.*[31] and the broadening of the peaks in Fig. 2 to roughly estimate the size of the particles, which are responsible for the peak broadening (''effective particle size''). The full width at half maximum (FWHM) intensity of both peaks in Fig. 2 increased from roughly 4 cm^{-1} for PL-5000 Å to 9 cm^{-1} for IF-200 Å. Consequently, the uncertainty in the phonon wave vector Δq causes a broadening of 5 cm^{-1}. From the dispersion curves presented by Wakabayashi *et al.*[31] we extract Δq by finding the largest q satisfying this uncertainty condition. By substituting the value of Δq deduced from the dispersion curve into

$$\Delta q = \frac{2\pi}{L} \tag{2}$$

it is possible to calculate the ''effective particle size'' L. We note that, following the layered compound approximation, both the E^1_{2g} and A_{1g} phonons are dispersionless in the Γ-A and Γ-L directions. Thus only the Γ-M and Γ-K dispersion curves are relevant, where the wave vector q ranges from 0 to $2\pi/a\sqrt{3}$.[31] Therefore, instead of Eq. (2), we use

$$L = 2 * \frac{2\pi}{\sqrt{3}} * \frac{1}{q}. \tag{3}$$

As a result of this argument, we found that the ''effective particle size'' causing the peaks to broaden from 4 to 9 cm^{-1} [Fig. 2(g)] to be roughly 100 Å. The fact that a 100-Å coherence length for the phonons was calculated from the RR spectra of IF particles 200 Å in diameter indicates that in the case of the IF phase, the broadening is not correlated to the particle size. Nevertheless, as the IF particle size increases to 800 Å [Fig. 2(d)] the FWHM decreases. The TEM examinations showed that IF nanoparticles 300 Å in diameter contain facets 70-250 Å long [Fig. 1(a)]. For smaller IF nanoparticles (200 Å), it is reasonable to estimate an average facet length of 100 Å. Therefore, we conclude that the broadening of the FOR modes in IF-MoS_2 particles is due to the confinement of phonons by the grain boundaries of the facets. As the IF particle size increases, the average facet length increases up to ~350 Å and the FWHM decreases [Fig. 2(c)]. Accordingly, the first-order modes of the 300 Å PL nanoparticles [Fig. 2(e)] are slightly broader than those of the 800-Å IF [Fig. 2(d)] and of the 1000-1500 Å nanoparticles [Fig. 2(c)], but the FWHM of larger size PL [500 Å Fig. 2(b)] is smaller than that of all IF samples.

In the room-temperature RR spectra [Fig. 3(a)], in addition to the broadening of the two first-order modes, their relative intensities change from sample to sample due to the enhancement of the A_{1g} mode. The resonance condition in Raman spectroscopy arises when the laser excitation energy coincides with an electronic absorption band, causing an enhancement in the total scattering cross section.[32] However, different phonons (normal modes) display different degrees of enhancement, depending on their contributions to the electronic polarizability. Normal modes that modulate the electronic band gap strongly tend to have larger resonant Raman scattering cross sections.[32] By performing dynamic (electronic) band-structure calculations, we studied the coupling of specific normal modes to the electronic transitions in bulk moS_2. Brändle and co-workers[24] used the ''extended Hückel approximation'' procedure to calculate the electronic structure of a MoS_2 single layer, and found that the stacking of these layers with just van der Waals interactions between the slabs has only little influence on the result of the calculation. The smallest direct gap is situated at the K point of the BZ, and the smallest indirect gap goes from Γ to K, with values of the direct gap and indirect gap being 0.68 and 0.47 eV, respectively.[24] Although the MoS_2 single-layer band calculations are in good agreement with more sophisticated calculations, the calculated band gaps are too small. Brändle and coworkers[24] suggest that the band gaps could be adjusted by optimizing the Slater orbital coefficients. A MoS_2 single layer model was also used to calculate the phonon dispersion curves.[33] It was found that the zone-center phonons have almost the same frequencies as those calculated for MoS_2 bulk.[33]

The dynamic calculations show that when ''applying'' the A_{1g} mode to a MoS_2 single layer, both the direct and indirect gaps are strongly modulated. On the other hand, the E^1_{2g} mode couples only weakly to the electronic structure. These calculations are in good agreement with the observed resonance enhancement of processes involving the A_{1g} mode, when the excited laser line is close in energy to the direct band gap and to the exciton (1.96 and 1.88 eV, respectively). We suggest that, since the character of the direct electronic transition final state K_5 is mainly associated with Mo d^2_z atomic orbitals aligned along the c axis,[15] and the A_{1g} pho-

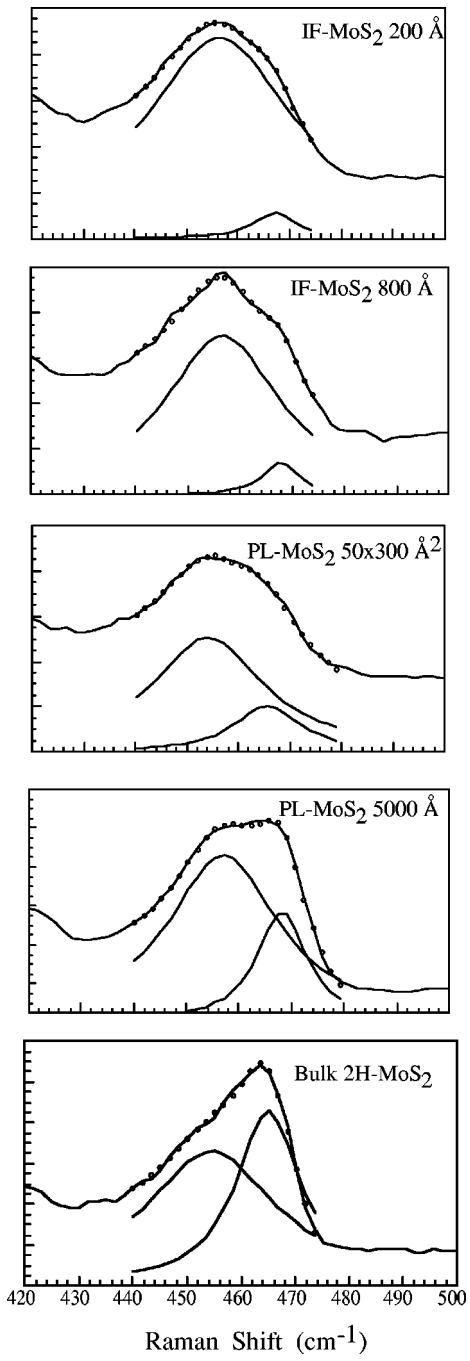

FIG. 5. A line-shape analysis of the $\sim$460-cm^{-1} feature in the RT RR spectra of different MoS_2 samples. The circles represent a line fitting to the spectra. The fitted data and Lorentzian functions are used in order to deconvolve the feature into two peaks. The resulting two peaks are presented below the experimental data for each sample.

non includes atomic displacements in the *c*-axis direction, a strong electron-phonon coupling along the *c* axis occurs under resonance conditions.

Figure 3(a) shows that the A_{1g} mode experiences more enhancement in the RR spectra of the nanoparticles [curves *a*–*c* in Fig. 3(a)] than in the RR spectrum of the single crystal [curve *e* in Fig. 3(a)]. This observation can be attributed to the characteristics of the electronic density of states (DOS) in the nanoparticles and in the single crystal, as predicted by a simple particle in a boxtype model.[1] For the single crystal, the DOS is constructed from a continuous distribution of levels, while the DOS of the nanoparticles has a more discrete distribution of states. Therefore, the coupling of the A_{1g} mode to a specific electronic state in the DOS is stronger in the case of the nanoparticles, resulting in a stronger resonance effect.

The relaxation of the $q=0$ selection rule due to the defects of finite crystallite size not only broadens the Raman-allowed modes, but can also cause new modes to appear which correspond to $q\neq 0$ phonons. For example, the disorder-induced peaks near 1350 and 1620 cm^{-1} observed in the Raman spectra of finite-size graphite particles using 5145-nm laser energy excitation[34,35] have been assigned to intense features in the phonon density of states appearing near these phonon energies.[36] In the graphite dispersion relations, optical phonon bands associated with regions about the *K* and *M* points of the hexagonal BZ produce peaks in the density of states near $\sim$1250 and 1350 cm^{-1}, respectively. Accordingly, with decreasing MoS_2 particle size and increasing disorder, additional peaks are expected to appear at frequencies corresponding to a large density of states produced by zone-edge phonons.[32]

In the RR spectra of the MoS_2 nanoparticles [curves *a*–*c* in Fig. 3(a)], in addition to the peaks observed for the single-crystal samples, new modes are observed. An intense mode is located at 226 cm^{-1}. Previous inelastic neutron scattering (INS) data showed that the frequency of the rigid-layer E_{2g}^2 mode at the Γ point increases as q moves away from the Γ point in the Γ-M direction, to reach the longitudinal acoustic mode LA(M)$\approx$232 cm^{-1} [where LA(M) denotes the phonons on the LA branch near the *M* point in the Brillouin zone].[31] Lattice dynamic calculations found the LA(M) mode to be at 228.4 cm^{-1}.[22] Therefore, we suggest that the appearance of the 226-cm^{-1} feature in MoS_2 is similar to that of the 1350-cm^{-1} peak in small crystallite graphite systems, as described above. Namely, the peak in the density of phonon states, which is found near the frequency of $\sim$230 cm^{-1},[31] is the primary source of this Raman band that appears only in the nanoparticle samples. Although *K*-point acoustic phonons may contribute, calculations of zone-edge frequencies[33] show that the *K*-point LA phonon is about 30 cm^{-1} lower in frequency than that of the *M*-point LA phonon. The possibility of impurity contaminants as the source of this feature is ruled out due to the high purity of the MoO_3 precursor[12] and the fact that the strong MoO_3 Raman bands lie outside of the 200-240-cm^{-1} frequency range.[37]

Furthermore, if the 226-cm^{-1} peak were due to a two-phonon difference combination process in which a phonon is annihilated (similar to the 180-cm^{-1} peak), it would have to be strongly dependent on temperature. A difference process, which creates one phonon (ω_2) and absorbs another phonon (ω_1), has a temperature dependence of the form[19]

$$n(\omega_1,T)[n(\omega_2,T)+1], \tag{5}$$

where $n(\omega,T)=(e^{h\omega/kT}-1)^{-1}$ is the phonon occupation probability that phonons of frequencies ω_1 and ω_2 are absorbed and created, respectively. A rough estimate shows that if the 226-cm^{-1} peak were due to a combination process, then the intensity at 125 K would be a factor of $\sim$7 lower than the intensity at room temperature, so that the 226-cm^{-1}

TABLE IV. The positions and relative intensity (third column/fourth column) of the two fitted peaks for the different MoS_2 samples at room temperature (RT) and 125 K.

Temperature (K)	Sample size (Å)	Peak position (cm^{-1})	Peak position (cm^{-1})	Relative intensity
300	2*H*-bulk (#1)	454.5	465.0	1.6
300	2*H*-bulk (#2)	455.4	464.1	1.9
300	PL-5000	457.1	468.1	3.3
300	IF-1500	451.3	462.7	7.8
300	IF-800	456.7	468.0	16.4
300	IF-200	456.4	467.1	27.7
300	PL-50×300	451.3	462.3	5.2
125	2*H*-bulk (#1)	459.5	466.2	1.6
125	PL-5000	458.2	467.2	1.5
125	IF-1500	456.4	466.5	2.3
125	IF-800	457.6	467.0	1.9
125	IF-200	457.7	467.4	2.2

feature would not be expected to be seen at 125 K. In contrast, the intensity of a first-order phonon should show little temperature dependence.

Figure 3(b) shows the low-temperature (125 K) Raman spectra of MoS_2 single crystal and nanoparticles [same samples as shown in Fig. 3(a)]. As expected, the 180-cm^{-1} peak, which is attributed to a combination process, is absent from all the spectra at 125 K. Nevertheless, the 226-cm^{-1} peak is still observed in the nanoparticle spectra at low temperature. Thus, we believe that the disorder-induced peak observed at 226 cm^{-1} is due to first-order scattering of LA(M) phonons.

Inclusion of disorder could also be the cause for the appearance of the other new peaks at 247 and 495 cm^{-1}, in that the 247-cm^{-1} peak corresponds to scattering of a zone-edge phonon, while the peak at 495 cm^{-1} would correspond to a second-order scattering process involving two such zone-edge phonons. Phonon dispersion and density of phonon states calculations[31] have shown that a peak in the density of phonon states due to a low-lying TO branch could fall in the range 250–300 cm^{-1}, although inelastic neutron scattering (INS) experiments failed to measure the frequencies of such phonons due to geometrical constraints. Ultimately, further neutron studies spanning a larger fraction of the BZ would be necessary to establish whether the 2*H* MoS_2 material supports a high density of phonon frequencies near 250 cm^{-1}.

Previous resonance Raman[21,22] (RR) studies assigned the intense ~460-cm^{-1} peak in crystalline MoS_2 as a second-order process involving the LA(M) phonon. Furthermore, many of the peaks in the RR spectrum of MoS_2 are assigned to sum or difference bands involving other phonons at the M point coupled to this LA(M) mode.[19,21] From the SOR spectra, Stacy *et al.*[21] were able to estimate the frequencies of the M-point optical modes corresponding to the branches associated with the zone center A_{1g} and E^1_{2g} modes.

In this paper, we suggest that the asymmetric feature at ~460 cm^{-1} in the RR spectra of MoS_2 single crystal is due to a combination of two peaks. A line-shape analysis (Fig. 5) shows that a doublet with the two peaks centered at 454 and 465 cm^{-1} constitutes this feature. Considering the observation of the 226-cm^{-1} mode in the RR spectrum of the nanoparticles and its identification with the LA(M) mode, we assign the 454 cm^{-1} peak to the second-order process of the zone-edge phonon 2LA(M). Accordingly, we expect the frequency of the single-crystal LA(M) mode to be 227 cm^{-1}, similar to the value observed for the nanoparticles. Using the same arguments and notation used in Ref. 21, we can deduce the frequencies of various BZ edge phonons. The frequencies and assignments of the various modes obtained for the MoS_2 single crystal and nanoparticles are tabulated in Table I.

Prior to this paper, the asymmetry of the ~460-cm^{-1} peak was assigned to the inverse parabolic shape of the LA(M) dispersion curve near the M point in the BZ.[21] In our analysis, we show that this peak is a combination of the second-order mode centered at 456 cm^{-1} and an additional peak centered at 466 cm^{-1}, which was not discussed in earlier studies. Although group theory does not predict a Raman-active mode at 466 cm^{-1}, a strong band appears at 466 cm^{-1} in infrared measurements.[38] This mode is assigned to the optical A_{2u} mode, which involves asymmetric translations of both Mo and S atoms in the c-axis direction. INS studies[31] and lattice dynamics calculations[22] have both shown the A_{2u} mode to be near 470 cm^{-1}. Wieting and Yoffe[39] studied the photoconductivity of MoS_2 and interpreted the spectral shift of the photoconductivity peak away from the exciton resonance in 2*H*-MoS_2 by means of an exciton-phonon ionization model. A dipolar phonon of energy 0.06 eV was required to account for a shift of 0.01 eV in the photoconductivity peak. Wieting and Verble[18] suggest that this shift can be explained by the A_{2u} phonon, which has an energy of 0.058 eV (~466 cm^{-1}). Moreover, it was pointed out[18] that the A_{2u} phonon modulates the thickness of the layers and should therefore interact strongly with delocalized excitons. As a result of these observations and due to the fact that the Raman spectra excited at 6328 Å (1.96 eV) are under resonant conditions with the direct transition (and hence also with the A exciton), the 466-cm^{-1} feature observed in the Raman spectra could be assigned to the infrared-active A_{2u} mode. Although the A_{2u} mode is Raman inactive, under these resonance conditions the even symmetry exciton levels could mediate the scattering of this phonon.

Following the assignments of the two components consti-

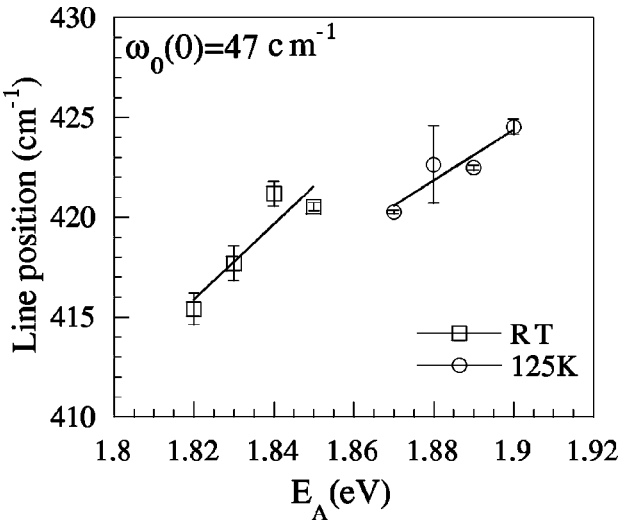

FIG. 6. Line position of the two-phonon ~420-cm^{-1} peak observed in MoS_2 plotted as a function of E_A, the A exciton energy. The solid lines represent the theoretical predictions for $\omega_0(0) = 47\ cm^{-1}$.

tuting the ~460-cm^{-1} feature to a second-order zone-edge scattering process and a first-order resonance-induced mode, their relative intensities are studied as a function of temperature and particle size. The relative intensities, $2LA(M)/A_{2u}$, calculated from the line-shape analysis of the spectra presented in Figs. 3(a) and 3(b), are given in Table IV. The $2LA(M)$ mode is enhanced relative to the A_{2u} mode as the nanoparticles size decreases at both 300 and 125 K. This enhancement of the $2LA(M)$ mode in the spectra of the nanoparticles is in good agreement with the observation of the first-order $LA(M)$ mode in the same spectra. Namely, the disorder in the PL and IF structure induces scattering from the zone-edge M point, hence, causing the appearance of the first-order zone-edge phonon in the RR spectra and causing the second-order scattering process to be enhanced. However, this enhancement of the $2LA(M)$ mode is expected to decrease at low temperature, since it is a zone-edge second-order process. The Raman line for the A_{2u} mode, on the other hand, is caused by a first-order process and is, therefore, temperature independent. As anticipated, although the $2LA(M)$ mode is still enhanced in the spectra for the nanoparticles at 125 K, the relative intensities are decreased compared to that observed at room temperature. Therefore, the dependence of the $2LA(M)$ and A_{2u} relative intensities of the $2LA(M)$ to the A_{2u} mode on the temperature and particle size support our assignments of these modes.

Due to quantum confinement, each of the samples studied possesses a different exciton energy E_{1s}^A, depending on the number of sulfide layers in the nanoparticle.[14] This change in electronic properties can be indirectly studied through its influence on the SOR scattering process, which produces a dispersive peak near 429 cm^{-1}. Figure 6 shows a plot of the position of this peak versus E_{1s}^A for several MoS_2 nanoparticle samples, and the results show a phonon frequency downshift for decreasing exciton energies. Sekine *et al.*[20] previously studied the RR spectra of MoS_2 bulk crystals in the laser frequency range of $1.9 < E_L < 2.3$ eV and showed that the highly dispersive band near 429 cm^{-1} could be explained as a second-order Raman process involving the scattering of a longitudinal quasiacoustic phonon (Δ_2) and an E_{1u}^2 phonon at finite wave vector. Assuming that the exciton-polariton dispersion relations are parabolic, the resonance condition for the second-order process involving an exciton of wave vector k_z and transitional mass $M_\parallel^A$ (effective mass in the direction parallel to the c axis) scattered along the c axis, is given by

$$\hbar\omega_i = E_{1s}^A + \frac{\hbar^2 k_z^2}{2M_\parallel^A} + \hbar\omega_0(q_z), \tag{6}$$

where $\hbar\omega_i$ is the incident laser energy, E_{1s}^A is the $1s$ exciton level, and $\hbar\omega_0(q_z)$ represents the dispersion of the quasiacoustic (Δ_2) phonon of wave vector q_z along Γ-A. We adopt the form $\omega_0(q_z) = \omega_0(0)\cos(|q_z|l_c/4)$ for the dispersion of the Γ-A branch, where l_c is the c-axis lattice constant (12.3 Å) and $\omega_0(0)$ is the frequency of the LO quasiacoustic mode at the Γ point (i.e., the B_{2g}^2 silent mode of MoS_2). Inserting this relation into Eq. (6) and considering crystal momentum conservation, we obtain

$$n_0\omega_i = c(|k_z| - |q_z|) \tag{7}$$

for MoS_2 which has an index of refraction $n_0 \approx 2.6$.[40] We are thus able to express the Raman shift of the $E_{1u}^2 - QA$ quasiacoustic phonon in the SOR scattering process in terms of the energy E_{1s}^A. A good fit to the aforementioned dispersive mode theory is obtained using $M_\parallel^A = 1.3m_0$[11] and $\omega_0(0) = 47\ cm^{-1}$, as shown in Fig. 6.

The value of $\omega_0(0)$ was found to be less than that found by both Sekine *et al.* (49 cm^{-1}) using RR scattering,[20] and by Wakabayashi *et al.* (56 cm^{-1}) using neutron scattering data.[31] A slight softening of this mode is consistent with the 2–4% c-axis lattice expansion previously observed in IF-MoS_2,[10] since the quasiacoustic B_{2g}^2 mode involves the vibration of S-Mo-S planes against each other, the frequency of which should go roughly as $\sim 1/l_c^2$.[41]

CONCLUSIONS

The Raman and resonance Raman spectra of MoS_2 nanoparticles, in the form of IF and PL, show a close correspondence to those of the bulk. Nevertheless, the first-order modes off resonance are broadened, and under resonance conditions new modes are observed. Since the IF particles are strongly faceted, we conclude that the ions can relax to their equilibrium positions, resulting in similar force constants to those for bulk crystals, and we further conclude that the phonons are confined by the boundaries of the facets. This confinement causes an uncertainty in the wave vector of the phonons, which results in broadening of the Raman features. Under resonance conditions, several peaks are observed in the Raman scattering spectra of the nanoparticles. From temperature-dependent RR measurements, it is possible to assign the intense new Raman feature at 226 cm^{-1} to FOR scattering of zone-boundary phonons activated by facet disorder. The RR study of the nanoparticles revealed that the intense ~460 cm^{-1} mode in the spectra of MoS_2 bulk and nanoparticles is a superposition of two peaks centered at 456 and 465 cm^{-1}. The lower frequency peak is assigned to the $2LA(M)$ process, while the upper frequency peak is as-

signed to the Raman inactive A_{2u} mode, which is activated by the strong resonance effect. Dynamic band calculations show that the coupling of the A_{1g} mode to the direct electronic transition is responsible for the enhancement of the A_{1g} mode under resonance conditions. Finally, studying the position of the dispersive band at 429 cm^{-1} in several MoS_2 samples with different band gaps showed a softening of the Raman inactive B_{2g}^2 mode. Since the quasiacoustic B_{2g}^2 mode involves the vibration of S-Mo-S planes against each other, the slight softening of this mode is consistent with the 2–4% *c*-axis lattice expansion previously observed in IF-MoS_2 by XRD measurements.[10] Consequently, we expect the E_{2g}^2 rigid-layer mode in the IF material, which is currently under investigation, to show the same trend and to shift to lower energies.

ACKNOWLEDGMENTS

G.L.F. and R.T. wish to thank Dr. Philip Klipstein for helpful discussions. This work was supported by the Minerva Foundation (Munich), ACS-PRF (USA), US-Israel Binational Foundation, and Applied Materials-Weizmann Foundation. M.J.M., M.S.D., and G.D. acknowledge support from NEDO and from NSF Contract No. DMR 98-04734.

[1] A. P. Alivisatos, J. Phys. C **100**, 13 226 (1996).
[2] C. B. Murray, D. J. Norris, and M. G. Bawendi, J. Am. Chem. Soc. **115**, 8706 (1993).
[3] P. M. Ajayan and T. W. Ebbesen, Rep. Prog. Phys. **60**, 1025 (1997).
[4] R. Tenne, L. Margulis, M. Genut, and G. Hodes, Nature (London) **360**, 444 (1992).
[5] L. Margulis, G. Salltra, and R. Tenne, Nature (London) **365**, 114 (1993).
[6] M. Remskar, Z. Skraba, F. Cléton, R. Sanjinés, and F. Lévy, Appl. Phys. Lett. **69**, 351 (1996).
[7] M. Remskar, Z. Skraba, M. Regula, C. Ballif, R. Sanjinés, and F. Lévy, Adv. Mater. **10**, 246 (1998).
[8] P. A. Parilla, A. C. Dillon, K. M. Jones, G. Riker, D. L. Schulz, D. S. Ginley, and M. J. Heben, Nature (London) **397**, 114 (1999).
[9] L. Rapoport, Y. Bilik, Y. Feldman, M. Homyonfer, S. R. Cohen, and R. Tenne, Nature (London) **387**, 791 (1997).
[10] Y. Feldman, E. Wasserman, D. J. Srolovitz, and R. Tenne, Science **267**, 222 (1995).
[11] M. Hershfinkel, L. A. Gheber, V. Voltera, J. L. Hutchison, L. Margulis, and R. Tenne, J. Am. Chem. Soc. **116**, 1914 (1994).
[12] Y. Feldman, G. L. Frey, M. Homyonfer, V. Lyakhovitskaya, L. Margulis, H. Cohen, G. Hodes, J. L. Hutchison, and R. Tenne, J. Am. Chem. Soc. **118**, 5362 (1996).
[13] M. Homyonfer, B. Alperson, Y. Rosenberg, L. Sapir, H. Cohen, G. Hodes, and R. Tenne, J. Am. Chem. Soc. **119**, 2693 (1997).
[14] G. L. Frey, S. Ilani, M. Homyonfer, Y. Feldman, and R. Tenne, Phys. Rev. B **57**, 6666 (1998).
[15] R. Coehoorn, C. Hass, and R. A. de Groot, Phys. Rev. B **35**, 6203 (1987).
[16] J. V. Acrivos, W. Y. Liang, J. A. Wilson, and A. D. Yoffe, J. Phys. C **4**, L18 (1971).
[17] J. P. Wilcoxon and G. A. Samara, Phys. Rev. B **51**, 7299 (1995).
[18] T. J. Wieting and J. L. Verble, Phys. Rev. B **3**, 4286 (1971).
[19] J. M. Chen and C. S. Wang, Solid State Commun. **14**, 857 (1974).
[20] T. Sekine, K. Uchinokura, T. Nakashizu, E. Matsuura, and R. Yoshizaki, J. Phys. Soc. Jpn. **53**, 811 (1984).
[21] A. M. Stacy and D. T. Hodul, J. Phys. Chem. Solids **46**, 405 (1985).
[22] C. Sourisseau, F. Cruege, and M. Fouassier, Chem. Phys. **150**, 281 (1991).
[23] R. Hoffman, J. Chem. Phys. **39**, 1397 (1963).
[24] M. Brändle, G. Calzaferri, and M. Lanz, Chem. Phys. **201**, 141 (1995). The program was downloaded from the World Wide Web homepage of Professor G. Calzaferri at the University of Bern (http://iacrs1.unibe.ch/members/biconcedit.html).
[25] D. J. Srolovitz, S. A. Safran, M. Homyonfer, and R. Tenne, Phys. Rev. Lett. **74**, 1779 (1995).
[26] M. J. Lipp, V. G. Baonza, W. J. Evans, and H. E. Lorenzana, Phys. Rev. B **56**, 5978 (1997).
[27] X. S. Zhao, Y. R. Ge, J. Schroeder, and P. D. Persans, Appl. Phys. Lett. **65**, 2033 (1994).
[28] H. Richter, Z. P. Wang, and L. Ley, Solid State Commun. **39**, 625 (1981).
[29] T. Kanata, H. Murai, and K. Kubota, J. Appl. Phys. **61**, 969 (1987).
[30] W. H. Weber, K. C. Hass, and J. R. McBride, Phys. Rev. B **48**, 178 (1993).
[31] N. Wakabayashi, H. G. Smith, and R. M. Nicklow, Phys. Rev. B **12**, 659 (1975).
[32] M. Cardona, in *Light Scattering in Solids II*, edited by M. Cardona and G. Guntherödt (Springer-Verlag, Berlin, 1983), p. 19.
[33] S. Jimenez Sandoval, D. Yang, R. F. Frindt, and J. C. Irwin, Phys. Rev. B **44**, 3955 (1991).
[34] F. Tuinstra and J. L. Koenig, J. Chem. Phys. **53**, 1126 (1970).
[35] A. V. Baranov, A. N. Bekhterev, Ya. S. Bobovich, and V. I. Petrov, Opt. Spectrosk. **62**, 1036 (1987) [Opt. Spectrosc. **62**, 612 (1987)].
[36] R. J. Nemanich and S. A. Solin, Phys. Rev. B **20**, 392 (1979).
[37] R. Srivastava and L. L. Chase, Solid State Commun. **11**, 349 (1972).
[38] J. L. Verble and T. J. Wieting, Phys. Rev. Lett. **25**, 362 (1970).
[39] T. J. Wieting and A. D. Yoffe, Phys. Status Solidi **37**, 353 (1970).
[40] B. L. Evans and P. A. Young, Phys. Status Solidi **25**, 417 (1968).
[41] A. G. Bagnall, W. Y. Liang, E. A. Marseglia, and B. Welber, Physica B **99**, 343 (1980).